ACS Photonics

Article

pubs.acs.org/journal/apchd5

Third-Harmonic Generation Enhancement by Film-Coupled Plasmonic Stripe Resonators

J. Britt Lassiter,[†,‡] Xiaoshu Chen,[§] Xiaojun Liu,[†,‡] Cristian Ciracì,[†,∥] Thang B. Hoang,[†,‡,⊥] Stéphane Larouche,[†,‡] Sang-Hyun Oh,[§] Maiken H. Mikkelsen,[†,‡,⊥] and David R. Smith*[,†,‡,⊥]

[†]Department of Electrical and Computer Engineering, [‡]Center for Metamaterials and Integrated Plasmonics, and [⊥]Department of Physics, Duke University, Durham, North Carolina 27708, United States

[§]Department of Electrical and Computer Engineering, University of Minnesota, Minneapolis, Minnesota 55455, United States

[∥]Istituto Italiano di Tecnologia (IIT), Center for Biomolecular Nanotechnologies, Via Barsanti, I-73010 Arnesano, Italy

Supporting Information

ABSTRACT: Because of their ability to strongly localize and enhance optical fields, plasmonic nanostructures have the potential to dramatically amplify the inherent nonlinear response of materials. We illustrate the impact of this plasmonic interaction by investigating the third-harmonic generation (THG) from a system of film-coupled nanostripes operating at 1500 nm. Both the film and the stripes are gold, separated by a nanoscale layer of aluminum oxide (Al_2O_3) grown using atomic layer deposition. This nanoscale junction, with an ultrasmooth interface, forms a waveguide cavity resonator with a large and controllable electric field enhancement, whose plasmon resonance can be tuned independently by changing the stripe width. We study experimentally the dependence of THG on the field enhancement by varying the gap size between the stripe and the metal film while simultaneously maintaining a fixed plasmon resonance. The experiments are supported with numerical simulations in which nonlinear contributions of the dielectric spacer layer and the metal are considered. Enhancements of the THG of nearly 5 orders of magnitude with respect to a bare metal film are measured experimentally for the smallest gap sizes, with a trend similar to that found in the numerical simulations.

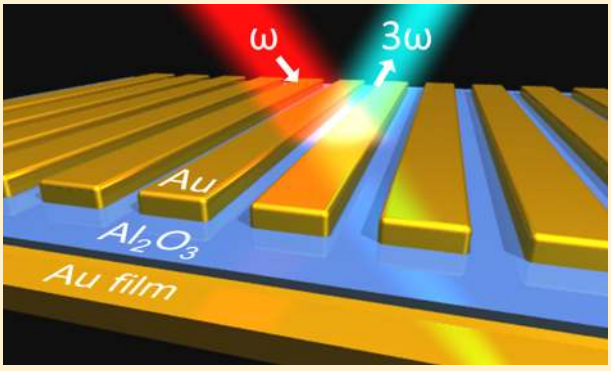

KEYWORDS: *third-harmonic generation, nonlinear optics, plasmonics, nanoantenna, patch antenna*

Nonlinear up-conversion of visible and infrared light to higher frequencies has been studied extensively and used in a variety of applications including biomedical imaging techniques[1−5] and higher energy coherent light sources.[6,7] While traditionally, nonlinear conversion has been limited to bulk crystalline materials that take advantage of phase matching, recently it has been shown that nanoscale plasmonic structures can also be used as media for nonlinear optics.[8] Various plasmonic structures have been explored for second-harmonic generation,[9−13] third-harmonic generation,[14−16] four-wave mixing,[17−19] and higher harmonic generation.[7,20] Because plasmonic nanostructures are smaller than the wavelength of light, phase matching cannot be exploited further; moreover, because plasmonic materials are often metals, it is difficult to access the inherent large third-order nonlinear susceptibilities that metals possess, with interactions confined to just the skin depth region of the metal. However, plasmonic structures do possess advantageous properties that can be exploited for nonlinear optics, such as large optical field enhancements[21,22] that can, in turn, substantially enhance many nonlinear processes.

In particular, when two plasmonic nanostructures are positioned in close proximity to each other, hybridization between the plasmon resonances inherent to each of the nanostructures can result in extremely large electric fields that build up between the nanostructures.[23−25] To achieve the maximum impact from the plasmonic effects, a large research emphasis has been placed on achieving the ultimate field enhancements in coupled nanostructures. Many of these geometries, such as chemically or lithographically fabricated dimers,[15,16,18,26] bowties,[7,27] and oligomer[13,17] structures have been explored for nonlinear optics. However, chemically synthesized cluster structures suffer from randomness in geometry and position, as well as limitations in yield, while lithographically fabricated clusters suffer from lower field enhancements due to difficulties in realizing precisely controlled nanometer-scale gaps between in-plane features.[28] Recently it has been shown that these fabrication limitations can be overcome and large field enhancements can be realized

Received: August 3, 2014
Published: October 21, 2014

ACS Publications © 2014 American Chemical Society

using film-coupled nanoparticles.[22,29,30] For the film-coupled nanoparticle system, the plasmonic junction is defined by planar deposition of materials, which allows for well-controlled nanometer-scale gaps and the ability to load the gaps with a wide range of materials.

In this paper, we study the third-harmonic generation (THG) enhancement of film-coupled nanostripes as a function of gap size. We employ lithographically fabricated gold stripes positioned over a gold film separated by a thin layer of Al_2O_3. Although the gold stripes are fabricated by lithography, our samples do not suffer from the feature size limitations typically associated with lithography because the plasmonic junctions are defined by atomic layer deposition (ALD) of the Al_2O_3. The resonance wavelength of each structure is fixed around 1500 nm by varying the gap size and the width of the stripes. We characterize the THG from these structures as a function of the gap size between the stripes and film, comparing the signal level to that of a bare gold film control sample. From this comparison, we show that the THG signal is enhanced by almost 5 orders of magnitude relative to that of the gold film. The experiments are supported with numerical simulations in which the contributions of both the gold and the Al_2O_3 spacer layer, formed using ALD, to the nonlinear enhancement are taken into account. We show that although Al_2O_3 has a relatively small third-order susceptibility, the THG is greatly enhanced due to the large field enhancements of the film-coupled nanostripes.

A schematic of the sample geometry used in this study is shown in Figure 1a. First, a 30 nm gold film was fabricated by template stripping.[31,32] This technique results in a gold film on a hardened optical epoxy (NOA 61, Norland Products Inc.) substrate with an ultrasmooth top surface. On top of the gold film, a thin layer of Al_2O_3 was deposited by ALD at 50 °C to define a plasmonic nanoscale junction between the Au film and the metal stripes deposited on top of the Al_2O_3 layer.[33,34] A periodic array of Au stripes were fabricated on top of the Al_2O_3 layer by electron beam lithography. The period between stripes was fixed at 250 nm, the height of the stripes was set at 30 nm, and the length was set at 50 μm. This geometry results in a coupled plasmonic structure that behaves as an optical frequency patch antenna such that the Al_2O_3 gap defines a waveguide cavity resonator where plasmons can propagate along the width and are reflected at the edges.[30,35] As a result, both the width, W, and the gap size, g, determine the plasmon resonance frequency. The width determines the cavity length, while the gap size determines the effective index in the waveguide. Here the electric fields are mostly confined inside the gap, and thus near-field coupling between the stripes is minimized. Six different samples were fabricated with gap sizes ranging from 2.83 to 11.40 nm. With all other geometric parameters fixed, increasing gap size blue-shifts the plasmon resonance, pushing the THG toward the UV range. The shifted plasmon resonance introduces an additional mechanism to the THG amplitude, since the material properties of the gold disperse as a function of wavelength. To eliminate any changes in the THG due to the material dispersion, we fix the resonance wavelength of each sample to 1500 nm by varying simultaneously the gap size and the width of the stripe. The variation of the stripe width affects only the resonance wavelength, while variation of the gap affects both the enhancement as well as the resonance wavelength. By studying film-coupled stripes with varying gap sizes at the fixed resonance wavelength of 1500 nm, we are able to directly correlate THG enhancement with field enhancement.

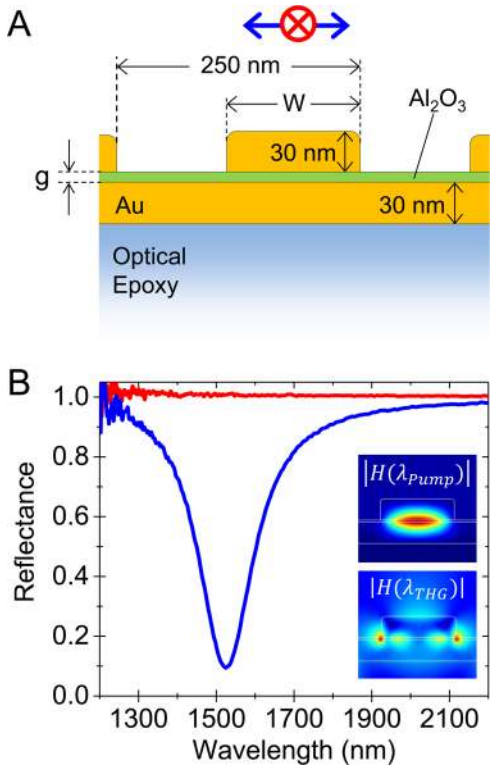

Figure 1. (A) Schematic of the plasmonic stripe geometry. (B) Representative polarized reflectance spectra of the thinnest gap sample (g = 2.83 nm). The blue (red) curves represent spectra taken with incident light polarized according to the blue (red) arrows in (A). Insets show the magnetic field profiles of the waveguide-cavity modes at both the pumping and third-harmonic generation (THG) wavelengths.

A representative reflectance spectrum, measured by Fourier transform infrared spectroscopy, is shown in Figure 1b for the sample with the smallest gap size (2.83 nm). When the polarization (electric field) of the incident field is oriented along the length of the stripe (transverse electric, or TE), no resonance is observed because the length of the waveguide is too long to support resonances in this wavelength range. For the opposite polarization (transverse magnetic, or TM), in which the electric field is oriented along the width of the stripe, a strong minimum approaching zero is observed in the reflectance spectrum near 1500 nm, indicating the film-coupled stripe behaves as a near-perfect absorber[36] where most of the photonic energy incident on the structures is coupled into the gap region. As a result, the electric field is drastically enhanced in the gap region with a maximum electric field at the edges of the stripe and maximum magnetic field at the center of the stripe, characteristic of a half-wavelength resonator (Figure 1b). For the g = 2.83 nm case, the enhancement of the electric field in the gap half way between the gold stripe and the gold substrate is 57. This large electric field is the determining factor for the enhancement of THG.

For each of the six samples, the desired width of the stripes was determined by the experimental requirement that the plasmon resonance be positioned near 1500 nm in wavelength. This requirement resulted in an increasing stripe width as the gap size was increased, in order to maintain a resonance near 1500 nm for all of the samples. The widths of the stripes were

dx.doi.org/10.1021/ph500276v | ACS Photonics 2014, 1, 1212−1217

measured by SEM to be 104, 119, 127, 153, 166, and 188 nm, respectively, in order of the thinnest to thickest gap samples. The reflectance spectrum for each sample is shown in Figure 2,

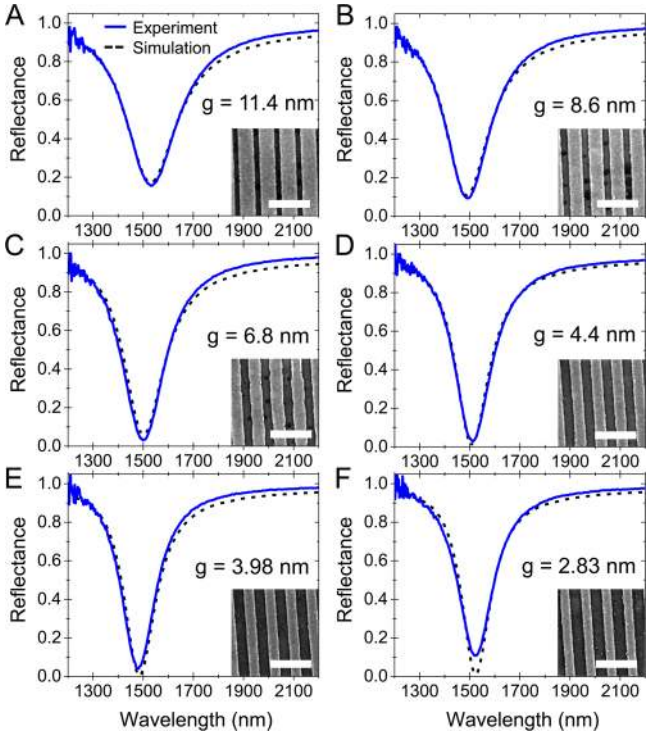

Figure 2. Experimental (blue) and simulated (black) reflectance spectra for each of the stripe samples used in the third-harmonic generation experiment. Each panel shows a representative spectrum from the sample with gap size indicated. Insets: SEM images of the stripe samples corresponding to the spectra (scale bar = 500 nm).

along with the simulated spectrum fitted to the experimental data. Each of the six experimental samples supported plasmon resonances within the range 1485 to 1530 nm. The simulated spectra were obtained using two-dimensional finite element method simulations (COMSOL Multiphysics) with periodic boundary conditions and plane wave illumination at normal incidence. The simulations were fitted to the experimental spectra by varying the gap size, while the other parameters remained fixed for each sample: stripe width measured by SEM, 30 nm stripe thickness, 30 nm gold film thickness, 250 nm period, and a 5 nm rounding radius on the top corners of the stripes. Although the rounding of the corners can be quite important in many geometries,[37] here the enhanced fields are confined mostly to the gap, so the rounding of the top corners did not have a significant effect. The thickness of the Al_2O_3 layer may differ slightly from the nominal values, and thus the final experimental gap sizes were determined by fitting the plasmonic spectra to simulations. The gap sizes were determined to be 2.83, 3.98, 4.40, 6.80, 8.60, and 11.40 nm. Because the gap size varies, but the resonance remains the same, the electric field in the gap increases with smaller gap sizes, enhancing the THG. By requiring the resonance to remain as close to the same wavelength as possible for all samples, we ensure that the effects of spectral dispersion in both the linear and nonlinear optical properties of the materials are minimized in our experiments.

In order to probe THG enhancement for these structures, we use a custom optical setup (Figure 3) that focuses ultrafast laser

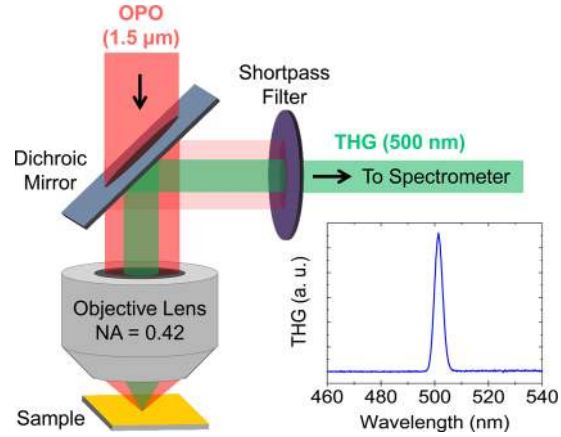

Figure 3. Schematic diagram of experimental setup for measurement of THG. Inset: representative THG spectrum measured from a film-coupled stripe sample.

pulses (~200 fs) from a tunable OPO source (Coherent, Chameleon) onto the sample using a broadband-corrected microscope objective (Mitutoyo Plan Apo NIR, 50×). The experiment is performed in a reflection configuration such that the microscope objective also collects the generated third-harmonic signal. The fundamental laser line is filtered out using a dichroic mirror and short-pass filters, and the THG signal is directed into a spectrograph/CCD (Acton sp2500i/Princeton Instruments 400 BR Excelon) for data collection and analysis. Each measurement of the THG from a sample was taken as a spectrum (Figure 3, inset), and the THG signal for each sample was defined as the peak of a Gaussian fit to the measured spectrum. For each of the six samples shown in Figure 2, the polarization of the laser was oriented along the width of the stripes and was tuned to be at the minimum of the reflection spectrum in order to be efficiently coupled into the plasmon resonance mode.

The experimentally measured THG signal for each sample is shown in Figure 4 (blue). For each sample, five different stripe patterns were exposed to the laser, and the THG signal was collected during a 300 s exposure. The mean of the signal recorded from the five different stripe patterns is shown, and the error bars represent one standard deviation. Because the system is nonlinear with laser power, and because the local gap fields exponentially increase for smaller gaps, it was not possible to find a laser power where THG could be measured and laser damage could simultaneously be avoided from all six samples. Instead, the samples were separated into two groups. The 11.40, 8.60, and 6.80 nm samples were exposed to a higher average power (112 μW), while the 2.83 and 3.98 nm gap size samples were exposed to a lower average power (45 μW) to prevent laser damage. The 4.40 nm gap sample was exposed to both incident powers in order to provide a means of normalizing between the two groups. The THG signals measured from the 2.83 and 3.98 nm samples were normalized by multiplying by the ratio between the measured signals from the 4.40 nm gap sample at both incident powers (18.19). This normalization is justified by measuring the incident power dependence of the THG signal from the 4.40 nm gap sample (Figure 4c). The THG signal power dependence is plotted on a log scale plot, and follows a power law (slope = ~3). By using this normalization, the trend for the dependence of the THG signal versus the gap size between the stripes and the metal film can be clearly observed. Further justification and discussion

dx.doi.org/10.1021/ph500276v | ACS Photonics 2014, 1, 1212−1217

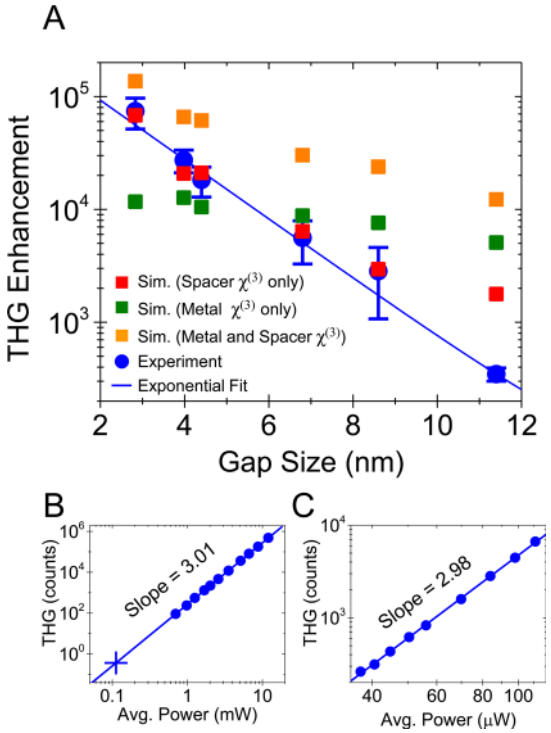

Figure 4. (A) Third harmonic generation enhancement (as compared to a bare gold film) vs gap size (g). (Blue) Experimentally measured THG enhancement, (red) numerically simulated THG enhancement that only takes into account the nonlinearity from the Al_2O_3 spacer layer. (Green) numerically simulated THG enhancement that only takes into account the nonlinearity from gold, (orange) numerically simulated THG enhancement taking into account the nonlinearities of both the gold and Al_2O_3 spacer layer. (B) Power dependence of the THG signal from a bare 30 nm gold film. (C) Power dependence of the THG signal from a stripe pattern on the g = 4.2 nm sample.

regarding this normalization is presented in the Supporting Information.

For the experimental data to be quantitatively compared to simulations, it must be expressed in terms of a known reference signal that is present and measurable in both simulation and experiment. We have chosen the THG signal from the background gold film as a convenient reference, and thus, all data points in Figure 4a are expressed as an enhancement with respect to a 30 nm template-stripped gold film (i.e., THG signal from the stripe sample divided by the THG signal from the bare gold film). For the experimental data, this reference THG signal was measured from a 30 nm bare gold reference sample fabricated by template-stripping in the same manner as the bottom layer of the film-coupled nanostripes samples but without the Al_2O_3 layer or the gold stripes. However, the THG signal is too weak to be observed from the bare gold sample at the same incident power level as was used for the stripe samples. Thus, in order to accurately express the data as an enhancement factor, the THG signal from the bare gold sample was measured as a function of incident power at higher powers where the signal could be observed (Figure 4b). The data were fitted to a straight line on the log scale plot (power law) with slope = 3.01. Because the fit is high quality (R^2 = 0.9999992) and the slope is approximately 3, we can extrapolate the fit function to the lower powers used to measure the stripe patterns (0.367 counts at an input power of 112 μW, indicated by the blue cross in Figure 4b). The experimental THG signal from the stripe samples were divided by this value in order to get the enhancement with respect to the background gold film, shown as the blue data points in Figure 4a. These enhancement values are beneficial because they can be quantitatively compared with similar enhancement values from numerical simulations.

The data appear to show a linear trend on the semilog plot suggesting an exponential increase in the measured THG signal with decreasing gap size. The blue line in Figure 4a represents a fit to the experimental data with an exponential function, $y = a + be^{-cx}$, where the fit parameters are a = 37, $b = 3.1 \times 10^5$, and c = 0.6. This trend is due to the increase in the electric field as the gap size is made smaller. Note that the volume of the gold and Al_2O_3 layers are also changing across the samples, and thus the conversion volume is also changing, but the signal actually decreases as the conversion volume increases. Because of this and because the volume changes are small as compared to the more than 2 orders of magnitude difference in signal between the largest and smallest gap samples, we can assume that any effect due to changes in the conversion volume is insignificant. For the 2.83 nm gap sample, the THG enhancement is measured to be 4.8 orders of magnitude greater than that from a bare gold film, indicating that this geometry is highly efficient at enhancing the THG. In order to understand these results, we performed nonlinear simulations of the structures using the commercial software COMSOL Multiphysics. For these simulations, third-harmonic fields were calculated by assuming that the fundamental fields are negligibly affected, undepleted pump approximation, by the up-conversion process. That is, the fields at the fundamental wavelength (λ) were used in the source term for computing the response at the third-harmonic wavelength ($\lambda/3$). Here, the permittivity of the 30 nm template stripped gold film and evaporated gold stripes were taken from empirical data,[38] and thus any absorption of the ~500 nm THG emission due to the interband transitions of gold was fully accounted for in our simulations. The $\chi^{(3)}$ used for calculating the THG from the bare gold film was 2.45×10^{-19} $(m/V)^2$, which is an orientational average of the $\chi^{(3)}$ tensor of polycrystalline gold film.[39] The $\chi^{(3)}$ for the gold in the film-coupled stripes is uncertain and could be a complex value.[40] However, we still took $\chi^{(3)} = 2.45 \times 10^{-19}$ $(m/V)^2$ as an approximation. Though the properties of $\chi^{(3)}$ for crystalline Al_2O_3 are well-known, the very thin, amorphous spacer layer may not necessarily have the same properties as larger bulk crystals. We therefore treated the spacer layer as an isotropic nonlinear material whose third-order nonlinear polarization was given by

$$\mathbf{P} = \frac{1}{4}\varepsilon_0\chi^{(3)}(\mathbf{E}\cdot\mathbf{E})\mathbf{E} \tag{1.1}$$

We then fitted the simulation results to the experimental measurements, finding a value of $\chi^{(3)}$ $(Al_2O_3) = 2.3 \times 10^{-23}$ $(m/V)^2$, which is relatively reasonable when compared to the $\chi^{(3)}$ ($\sim 10^{-22}$ m^2/V^2) of crystalline Al_2O_3.[41] As shown in Figure 4a, the fitted trend of the simulated THG as a function of gap size is in good agreement to that measured in the experiments, following an exponential increase with decreasing gap size. However, the fit in Figure 4a (red curve) does not account for the nonlinear contribution of gold in the structured samples.

Because the gold film and nanostripes both possess a relatively large $\chi^{(3)}$ that could potentially give rise to the observed THG, we performed a numerical study to investigate the THG that would arise from the gold alone. In Figure 4a, we

dx.doi.org/10.1021/ph500276v | ACS Photonics 2014, 1, 1212−1217

present a simulated THG curve that takes into account only the nonlinear contribution from the gold (green curve). In this case, the trend of the simulated THG as a function of gap size is distinct from that measured in the experiments. The trend observed in the simulations results from the limited field penetrating into the gold. When decreasing the gap size, the fields confined within the gap are stronger, as are the fields inside the gold; however, due to the large losses in gold, only the field near the gold surface is significantly enhanced. The trade-off between the field enhancement and loss mechanisms due to the gold nonlinearity results in a much flatter curve in Figure 4a (green curve). Note that the green curve exceeds the experimentally measured THG enhancement for gap sizes larger than 6 nm. One possible cause of this discrepancy is that our current models do not account for other possible nonlinear effects that can occur in this system. It is possible, for example, that competition between enhancement by the Al_2O_3 spacer layer and reduction by nonlinear absorption and other processes could account for the observed experimental enhancement values. It is also possible that nonlinear absorption could severely decrease the observed THG signal in simulation and hence bring both the green and the red curve down below the experimental curve. In Figure 4a, we also show the simulation result including both nonlinearities from the gold and the spacer layer (orange curve). The THG from the gold and the spacer interfere constructively, resulting in a total THG enhancement exceeding that from either the gold or the spacer alone. However, analyses regarding nonlinear absorption and the interference between different THG sources[42] are beyond the scope of this paper.

In conclusion, we have fabricated film-coupled nanostripe plasmonic antennas that support waveguide cavity resonances and measured the THG as a function of the gap size separating the stripes and the film. We observed a large THG enhancement of 4.8 orders of magnitude over the case of a bare gold film, and we have shown that this enhancement can be reasonably modeled using classical, local electrodynamic simulations. Our analysis indicates that the majority of the THG in these structures occurs inside the dielectric gap rather than in the metal, despite the relatively low $\chi^{(3)}$ value ($\sim 10^{-23}$) of the material inside the gap (Al_2O_3). However, it is difficult to distinguish the actual contributions of the metal and dielectric regions, and recent literature has shown that conclusions to this question can be contradictory, even for two very similar hybrid nanoantenna structures.[15,16] It is possible that other effects such as nonlinear absorption and interference between multiple THG sources account for a complete understanding of the observed THG signals, and additional work in this area is needed. Nevertheless, we have shown that the dielectric spacer layer plays a critical role, and thus the THG signal enhancement and the effective $\chi^{(3)}$ of the whole plasmonic structure could likely be drastically enhanced by using a material in the gap with a larger $\chi^{(3)}$. Because of the large observed THG enhancement and the ease with which the ultrasmooth gap can be loaded with different materials, the film-coupled stripe system has great potential for future nonlinear optics applications.

■ ASSOCIATED CONTENT

Supporting Information

Figures showing non-normalized THG data vs gap size and explanation of the normalization used for this data is presented. Figure and discussion of gap electric field compared to radiated THG. This material is available free of charge via the Internet at http://pubs.acs.org.

■ AUTHOR INFORMATION

Corresponding Author

*E-mail: drsmith@ee.duke.edu.

Notes

The authors declare no competing financial interest.

■ ACKNOWLEDGMENTS

This work was supported by the Air Force Office of Scientific Research (AFOSR, Grant No. FA9550-12-1-0491) and by the Army Research Office through a Multidisciplinary University Research Initiative (Grant No. W911NF-09-1-0539). X.S.C. and S.-H.O. acknowledge support from the DARPA Young Faculty Award (N66001-11-1-4152) and the Office of Naval Research Young Investigator Program (N00014-11-1-0645). T.B.H. and M.H.M. acknowledge support from the Lord Foundation of North Carolina.

■ REFERENCES

(1) Barad, Y.; Eisenberg, H.; Horowitz, M.; Silberberg, Y. Nonlinear scanning laser microscopy by third harmonic generation. *Appl. Phys. Lett.* **1997**, *70*, 922.

(2) Zipfel, W. R.; Williams, R. M.; Webb, W. W. Nonlinear magic: Multiphoton microscopy in the biosciences. *Nat. Biotechnol.* **2003**, *21*, 1369.

(3) Yellen, D.; Oron, D.; Thilberge, S.; Moses, E.; Silberberg, Y. Multiphoton plasmon-resonance microscopy. *Opt. Express* **2003**, *11*, 1385.

(4) Debarre, D.; Supatto, W.; Pena, A.-M.; Fabre, A.; Tordjmann, T.; Combettes, L.; Schanne-Klein, M.-C.; Beaurepaire, E. Imaging lipid bodies in cells and tissues using third-harmonic generation microscopy. *Nat. Methods* **2006**, *3*, 47.

(5) Tai, S.-P.; Wu, Y.; Shieh, D.-B.; Chen, L.-J.; Lin, K.-J.; Yu, C.-H.; Chu, S.-W.; Chang, C.-H.; Shi, X.-Y.; Wen, Y.-C.; Lin, K.-H.; Liu, T.-M.; Sun, C.-K. Molecular imaging of cancer cells using plasmon-resonant-enhanced third-harmonic-generation in silver nanoparticles. *Adv. Mater.* **2007**, *19*, 4520.

(6) Chang, Z.; Rundquist, A.; Wang, H.; Murnane, M. M.; Kapteyn, H. C. Generation of coherent soft X-rays at 2.7 nm using high harmonics. *Phys. Rev. Lett.* **1997**, *79*, 2967.

(7) Kim, S.; Jin, J.; Kim, Y.-J.; Park, I.-Y.; Kim, Y.; Kim, S.-W. High-harmonic generation by resonant plasmon field enhancement. *Nature* **2008**, *453*, 757.

(8) Kauranen, M.; Zayats, A. V. Nonlinear plasmonics. *Nat. Photonics* **2012**, *6*, 737.

(9) Bouhelier, A.; Beversluis, M.; Hartschuh, A.; Novotny, L. Near-field second-harmonic generation induced by local field enhancement. *Phys. Rev. Lett.* **2003**, *90*, 013903.

(10) Canfield, B. K.; Husu, H.; Laukkanen, J.; Bai, B.; Kuittinen, M.; Turunen, J.; Kauranen, M. Local field asymmetry drives second-harmonic generation in nanocentrosymmetric nanodimers. *Nano Lett.* **2007**, *7*, 1251.

(11) Zhang, Y.; Grady, N. K.; Ayaly-Orozco, C.; Halas, N. J. Three-dimensional nanostructures as highly efficient generators of second harmonic light. *Nano Lett.* **2011**, *11*, 5519.

(12) Butet, J.; Thyagarajan, K.; Martin, O. J. F. Ultrasensitive optical shape characterization of gold nanoantennas using second harmonic generation. *Nano Lett.* **2013**, *13*, 1787.

(13) Thyagarajan, K.; Butet, J.; Martin, O. J. F. Augmenting second harmonic generation using fano resonances in plasmonic systems. *Nano Lett.* **2013**, *13*, 1847.

(14) Lamprecht, B.; Krenn, J. R.; Leitner, A.; Aussenegg, F. R. Resonant and off-resonant light-driven plasmons in metal nano-

particles studied by femtosecond-resolution third-harmonic generation. *Phys. Rev. Lett.* **1999**, *83*, 4421.
(15) Aouani, H.; Rahmani, M.; Navarro-Cia, M.; Maier, S. A. Third-harmonic-upconversion enhancement from a single semiconductor nanoparticle coupled to a plasmonic antenna. *Nat. Nanotechnol.* **2014**, *9*, 290.
(16) Metzger, B.; Hentschel, M.; Schumacher, T.; Lippitz, M.; Ye, X.; Murray, C. B.; Knabe, B.; Buse, K.; Giessen, H. Doubling the efficiency of third harmonic generation by positioning ITO nanocrystals into the hot-spot of plasmonic gap-antennas. *Nano Lett.* **2014**, *14*, 2867.
(17) Zhang, Y.; Wen, F.; Zhen, Y.-R.; Nordlander, P.; Halas, N. J. Coherent Fano resonances in a plasmonic nanocluster enhance optical four-wave mixing. *Proc. Natl. Acad. Sci. U.S.A.* **2013**, *110*, 9215.
(18) Danckwerts, M.; Novotny, L. Optical frequency mixing at coupled gold nanoparticles. *Phys. Rev. Lett.* **2007**, *98*, 026104.
(19) Harutyunyan, H.; Volpe, G.; Quidant, R.; Novotny, L. Enhancing the nonlinear optical response using multifrequency gold-nanowire antennas. *Phys. Rev. Lett.* **2012**, *108*, 217403.
(20) Park, I.-Y.; Kim, S.; Choi, J.; Lee, D.-H.; Kim, Y.-J.; Kling, M. F.; Stockman, M. I.; Kim, S.-W. Plasmonic generation of ultrashort extreme-ultraviolet light pulses. *Nat. Photonics* **2011**, *5*, 677.
(21) Hao, E.; Schatz, G. C. Electromagnetic fields around silver nanoparticles and dimers. *J. Chem. Phys.* **2003**, *120*, 357.
(22) Ciraci, C.; Hill, R. T.; Mock, J. J.; Urzhumov, Y.; Fernandez-Dominguez, A. I.; Maier, S. A.; Pendry, J. B.; Chilkoti, A.; Smith, D. R. Probing the ultimate limits of plasmonic enhancement. *Science* **2012**, *337*, 1072.
(23) Aubry, A.; Lei, D. Y.; Maier, S. A.; Pendry, J. B. Interaction between plasmonic nanoparticles revisited with transformation optics. *Phys. Rev. Lett.* **2010**, *105*, 233901.
(24) Fernandez-Dominguez, A. I.; Zhang, P.; Luo, Y.; Maier, S. A.; Garcia-Vidal, F. J.; Pendry, J. B. Transformation-optics insight into nonlocal effects in separated nanowires. *Phys. Rev. B* **2012**, *86*, 241110(R).
(25) Pendry, J. B.; Aubry, A.; Smith, D. R.; Maier, S. A. Transformation optics and subwavelength control of light. *Science* **2012**, *334*, 549.
(26) Slablab, A.; Xuan, L. L.; Zielinkski, M.; Wilde, Y. d.; Jacques, V.; Chauvat, D.; Roch, J.-F. Second-harmonic generation from coupled plasmon modes in a single dimer of gold nanospheres. *Opt. Express* **2012**, *20*, 220.
(27) Hanke, T.; Krauss, G.; Trautlein, D.; Wild, B.; Bratschitsch, R.; Leitenstorfer, A. Efficient nonlinear light emission of single gold optical antennas driven by few-cycle near-infrared pulses. *Phys. Rev. Lett.* **2009**, *103*, 257404.
(28) Lindquist, N. C.; Nagpal, P.; McPeak, K. M.; Norris, D. J.; Oh, S.-H. Engineering metallic nanostructures for plasmonics and nanophotonics. *Rep. Prog. Phys.* **2012**, *75*, 036501.
(29) Mock, J. J.; Hill, R. T.; Degiron, A.; Zauscher, S.; Chilkoti, A.; Smith, D. R. Distance-dependent plasmon resonant coupling between a gold nanoparticle and gold film. *Nano Lett.* **2008**, *8*, 2245.
(30) Lassiter, J. B.; McGuire, F.; Mock, J. J.; Ciraci, C.; Hill, R. T.; Wiley, B. J.; Chilkoti, A.; Smith, D. R. Plasmonic waveguide modes of film-coupled metallic nanocubes. *Nano Lett.* **2013**, *13*, 5866.
(31) Hegner, M.; Wagner, P.; Semenza, G. Ultralarge atomically flat template-stripped Au surfaces for scanning probe microscopy. *Surf. Sci.* **1993**, *291*, 39.
(32) Nagpal, P.; Lindquist, N. C.; Oh, S.-H.; Norris, D. J. Ultrasmooth patterned metals for plasmonics and metamaterials. *Science* **2009**, *325*, 594.
(33) Chen, X.; Park, H.-R.; Pelton, M.; Piao, X.; Lindquist, N. C.; Im, H.; Kim, Y. J.; Ahn, J. S.; Ahn, K. J.; Park, N.; Kim, D.-S.; Oh, S.-H. Atomic layer lithography of wafer-scale nanogap arrays for extreme confinement of electromagnetic waves. *Nat. Commun.* **2013**, *4*, 2361.
(34) Ciraci, C.; Chen, X.; Mock, J. J.; McGuire, F.; Liu, X.; Oh, S.-H.; Smith, D. R. Film-coupled nanoparticles by atomic layer deposition: Comparison with organic spacing layers. *Appl. Phys. Lett.* **2014**, *104*, 023109.
(35) Ciraci, C.; Lassiter, J. B.; Moreau, A.; Smith, D. R. Quasi-analytic study of scattering from optical plasmonic patch antennas. *J. Appl. Phys.* **2013**, *114*, 163108.
(36) Moreau, A.; Ciraci, C.; Mock, J. J.; Hill, R. T.; Wang, Q.; Wiley, B. J.; Chilkoti, A.; Smith, D. R. Controlled-reflectance surfaces with film-coupled colloidal nanoantennas. *Nature* **2012**, *492*, 86.
(37) Raziman, T. V.; Martin, O. J. F. Polarisation charges and scattering behaviour of realistically rounded plasmonic nanostructures. *Opt. Express* **2013**, *21*, 21500.
(38) Olmon, R. L.; Slovick, B.; Johnson, T. W.; Shelton, D.; Oh, S.-H.; Boreman, G. D.; Raschke, M. B. Optical dielectric function of gold. *Phys. Rev. B* **2012**, *86*, 235147.
(39) Burns, W. K.; Bloembergen, N. Third-harmonic generation in absorbing media of cubic or isotropic symmetry. *Phys. Rev. B* **1971**, *4*, 3437.
(40) Boyd, R. W.; Shi, Z.; Leon, I. D. The third-order nonlinear optical susceptibility of gold. *Opt. Commun.* **2014**, *326*, 74.
(41) Boyd, R. W. *Nonlinear Opt.*, 3rd ed.; Academic Press: San Diego, 2008.
(42) Reinhold, J.; Shcherbakov, M. R.; Chipouline, A.; Panov, V. I.; Helgert, C.; Paul, T.; Rockstuhl, C.; Lederer, F.; Kley, E.-B.; Tunnermann, A.; Fedyanin, A. A.; Pertsch, T. Contribution of the magnetic resonance to the third harmonic generation from a fishnet metamaterial. *Phys. Rev. B* **2012**, *86*, 115401.